Universitat Politècnica de Catalunya (UPC)
Universitat Autònoma de Barcelona (UAB)
Universitat de Barcelona (UB)
Institut de Ciències Fotòniques (ICFO)

http://www.photonicsbcn.eu

Master in Photonics

MASTER THESIS WORK

CLOSED-LOOP CONTROL OF MAGNETIC FIELDS FOR ATOMIC PHYSICS EXPERIMENTS

Jie Luan

Supervised by Prof. Dr. Morgan Mitchell, (ICFO)

Presented on date 8th September 2017

Registered at

Escola Tècnica Superior d'Enginyeria de Telecomunicació de Barcelona

Closed-loop control of magnetic fields for atomic physics experiments

Jie Luan

ICFO The Institute of Photonic Sciences, Mediterranean Technology Park
Av. Carl Friedrich Gauss, 3, 009
Castelldefels (Barcelona), Spain

E-mail: jie.luan@icfo.eu

May - August 2017

Abstract. This project explores the control of magnetic fields through active feedback, ultimately bringing the magnetic field noise level below the required threshold, for one single axis. An absolute stability of less than 400 µG and repeatability better than 100 µG were achieved.

1. Introduction: physical background

A great variety of atomic phenomena require precisely-controlled magnetic field environments, including spinor dynamics in Bose-Einstein condensates (BEC) [1] and operation of ultrasensitive atomic sensors [2]. Solutions have been proposed, including passive shielding using nested layers of mu-metal shields [3] and active compensation [4]. In our lab we are running two experiments that require stable magnetic fields. First, the test of the atomic magnetometer's performance needs to be able to neglect the uncertainties induced by the external fields' fluctuations and thus evaluate only the uncertainty of the magnetometer [5]. Second, we want to explore the phase diagram in [1] for low magnetic fields and study spontaneous symmetry breaking. This needs a good repeatability in the radio frequency (RF) and microwave (MW) transitions [6] and therefore a stable magnetic field.

The quantization axis of the system is defined by a constant bias field of 286 mG, corresponding to a Zeeman shift of 200 kHz [6]. Under this condition, the atomic spins will precess about the bias field with the so-called Larmor frequency $\omega_L = 2\pi \cdot 200$ kHz. A field stability of less than 1 mG is required for a reliable operation of the RF and MW transitions used in the atomic state preparation.

In our experiment we already have passive control (three pairs of Helmholtz coils) for canceling out the quasi-static magnetic field (from Earth and other sources) and establishing the constant quantization field of 286 mG and a pair of anti-Helmholtz coils for establishing a field gradient [7]. However, we do not have an active control for canceling the AC fluctuating field as the one detected in our experiment (Fig. 7). Such 50 Hz noise comes mostly from power lines and power supplies in the neighborhood of the experiment.

In this project we propose implementing a closed-loop control system to stabilize the magnetic field. We start by introducing the assumptions that will simplify the analysis of the problem (Sec. 2). After, we comment on the construction and test of a miniaturized system. Sec. 3 presents in detail each of the designed components. Finally, magnetometry using ultra-cold atoms will be introduced (Sec. 4) to measure the compensation system's performance, discussed in Sec. 5.

2. Initial considerations

Our ultimate goal is to stabilize the magnetic field for the location where the atoms are found in the physical experiment. However, the experimental setup makes the neighboring space of the atom inaccessible, so we can only place the sensor next to the vacuum chamber, an all-glass, 9-window octagonal enclosure of 10 cm radius. In addition, two assumptions have to be made:

- The atoms experience the same field strength than the location where we place the sensor.
- The magnetic field we produce using compensation coils is the same at both sensor's position and vacuum chamber's center.

We argue the validity of the first point by noting that all the sources that produce a changing magnetic field are located at at least one meter from the atoms. The other important sources which we cannot control, such as the elevator's motor and the vacuum bombs from other labs, are far from our lab, thus they do not constitute any concern either. In [8], an array of six single-axis magnetic sensors was used to interpolate the field at the trap center. We opted for not implementing such system, just for simplicity. On the other hand, the second point can be proved by calculating numerically the magnetic fields the coils will produce on the two spots and checking that they are the same. Fig. 2 illustrates the calculated magnetic field for a square configuration we will explain in detail later. It shows that the field deviations are below 410 µG.

The validity of the two assumptions imply that we can stabilize the field at the atoms' vicinity by stabilizing the field at the sensor.

3. The components

The closed-loop control system starts with the sensor which detects the magnetic field strength along one axis. It converts the field strength into a voltage signal which is compared with a reference value. The PID controller calculates the difference between the reference and the input voltage and feeds an output voltage to the current driver which supplies a current to the coils. Finally the loop closes with the sensor detecting the combined field from both the noise and that produced by the compensation coils. When reaching convergence, such combined field would ideally be constant. Three such configurations are needed in order to stabilize the magnetic field along all three axes. Due to the limited time available, in this project we only implement and test the performance of one such configuration, detailed as the following.

3.1. The magnetic field sensor

The sensor we use to measure the magnetic field for compensation is a Mag-03 three-axis fluxgate magnetometer with a bandwidth of 3 kHz, measuring range of $\pm 1000\,\mu\mathrm{T}$, and noise levels down to $< 6\ \mathrm{pT_{rms}}/\sqrt{\mathrm{Hz}}$ at 1 Hz. The detected magnetic field signal outputs a voltage with scaling factor of $100\,\mathrm{mV}/\mu\mathrm{T}$. The inherent ± 5 nT offset in zero field is negligible for our measurements. We check the correct functioning of the sensor by measuring the Earth's magnetic field to be about 500 mG, as well as measured the sensor's Bode diagrams agreeing with the datasheet [9].

From what is detailed in [10] and [11], in essence, a fluxgate magnetometer consists of a pair of coils, namely drive and sense coils, wrapped around a highly magnetically permeable material and produce a induced voltage proportional to the magnetic field being detected. In comparison with previous realizations (as in [12]), we chose to use fluxgate magnetometer due to its enhanced sensitivity and low drift.

3.2. The current driver

We use a common source with source degeneration [13] configuration for driving the magnetic field coils.

The current driver's circuit is presented in Fig. 1. The Op-Amp-1 serves as an adder, it outputs the control voltage $\mathrm{V_{in}}$ plus an offset voltage $\mathrm{V_{offset}}$ which is larger than the gate-source threshold voltage for making a conductive channel, so the MOSFET (SiHG24N65E from Vishay Siliconix [14]) is turned on and a current is established between the drain and the source. This current is then fed into the coils, connected in parallel with a transient voltage suppressor (TVS) diode, which protects the circuit against overvoltages. The current can be monitored by reading the voltage value on the $1\,\Omega$ resistor, so the Op-Amp-2 is merely an amplifier for this voltage signal.

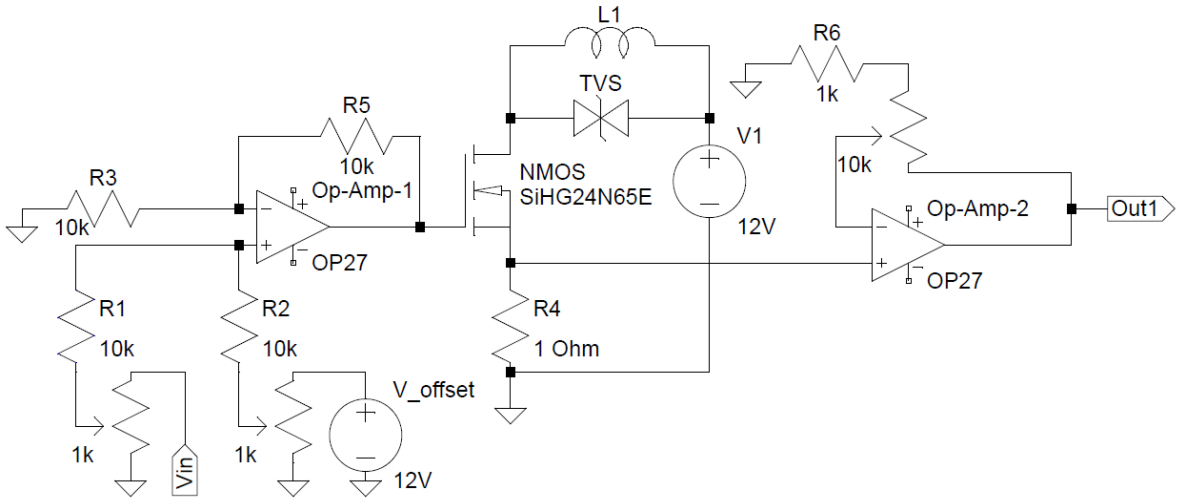

Figure 1: The circuit for the current driver.

3.3. The coils

First we characterized the small coils, of diameter 8 cm and separated 9 cm apart. We wrote a set of programs to acquire data from a Red Pitaya board, with 125 Ms/s rate, to plot the Bode diagrams of the coils (refer to the annexed codes `plot_bode.py`, `plot_functions.py` and `wave_functions.py` for more details). Its cut-off frequency (24 kHz) is well above the bandwidth of the sensor (3 kHz), so the speed at which the whole system responds is still limited by the sensor. Furthermore, with a curve fitting function we determined the value of the coils' inductance to be 0.35 mH.

Once we had the system working to control the small coils, we placed all the components close to the real atomic experiment, substituting the small coils by larger ones. We explored the different possibilities to provide an approximately uniform field for the central region where the atoms are located. We focused on rectangular coils, because they provide uniform magnetic field in larger volume [15]. We started by designing a cubic structure for simplicity. However, in analogy to circular coils, the advantages of the Helmholtz configuration can also be achieved in square coils by adjusting their spacing to 0.5445 times the length of a side [16]. Unfortunately we were unable to implement this configuration for all three pairs because that would imply perforating the optical table. As an alternative, we implemented it for one pair and chose slightly deviation spacings for the other two (not implemented in this project). Program `B_comp.py` plots the variation of the magnetic field along the axes (Fig. 2).

For the purpose of our noise cancellation requirement, we built a pair of square coils, with a side length of 1.46 m, by winding up to 40 turns of 22 AWG copper wire on an aluminum ITEM frame. The measured inductance (14 mH) was close to the estimated (12 mH, calculated using `L_comp.py`).

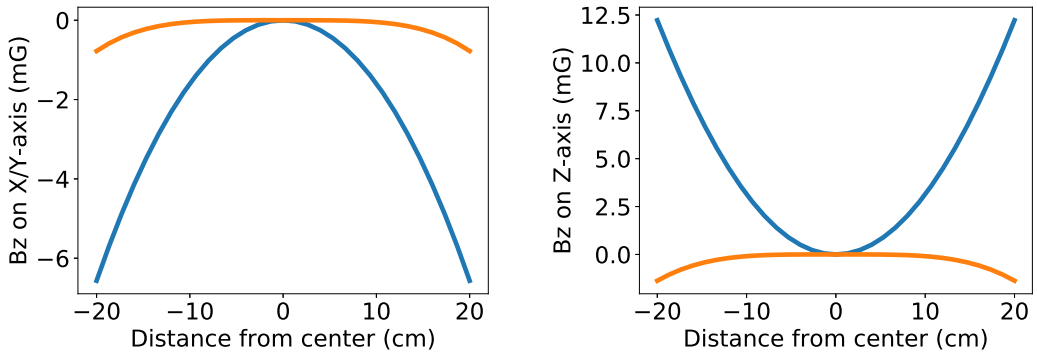

Figure 2: Field strength (difference with the central value) along the X and Y axes (left), and Z axis (right), calculated for 0.8 A current, 1.46 m side-length and 40 turns of wire per each coil. The magnetic field at the center is 202 mG in cubic configuration (blue) and 350 mG in Helmholtz configuration (orange).

3.4. The PID controller

A PID controller stabilizes the output signal of a process around a certain reference level. First it calculates the *error* signal as the difference between the *output* and the *reference*. Then it multiplies the error, its integral and its derivative by three different parameters namely K_p, K_i and K_d, respectively (hence the name of the controller), and adds the results. Finally it acts on the process using the *action* signal $u(t) = K_p e(t) + K_i \int_0^t e(\tau)d\tau + K_d \frac{de(t)}{dt}$ and the process output feeds back to close the loop.

Feedback solutions for magnetic field active compensation have been implemented as early as 1961 [17]. In our case, the *reference* is a constant voltage, which is equivalent to a constant magnetic field through the 100 mV/µT factor. The PID controller (script `PID.ino` available in the annex), implemented in a ChipKIT uC32 microcontroller (MCU) board [18] supplemented with an analog shield of 16 bit 100 ks/s rate [19], provides a voltage (the signal $u(t)$) to the circuit specified in the previous section. The coils then produce a magnetic field. Finally the sensor detects the field and outputs a voltage, again, using the 100 mV/µT factor. This voltage is fed into the PID controller thus closing the loop. The block diagram is shown in Fig. 3

We manually tuned the parameters K_p, K_i and K_d in order to optimize the compensator in terms of having less rise time, overshoot, settling time, steady-state error, but more stability. A combination of $K_p = 0.4$, $K_i = 0.3$ and $K_d = 0$ was established. Afterwards we measured the Bode diagrams of the whole compensating system (Fig. 4). The bandwidth of 1 kHz is far above the first harmonics of 50 Hz we want to compensate.

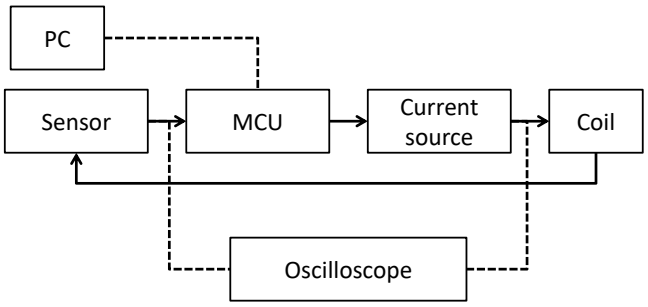

Figure 3: The compensator system's block diagram, with the PID controller implemented in the MCU. The MCU is controlled by a PC and the oscilloscope monitors the sensor's signal and the output current.

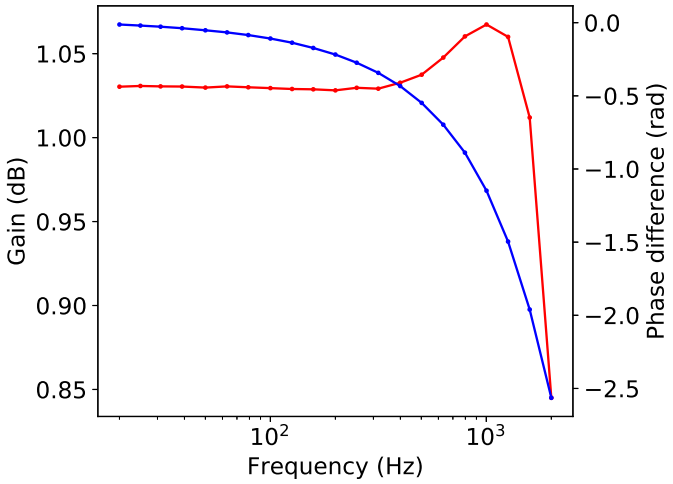

Figure 4: Bode diagrams of the compensator. Gain is plotted in red and phase difference in blue. Solid lines are guides to the eye.

4. Magnetometry with ultra-cold atomic ensembles

We directly used the ^{87}Rb atoms evaporatively cooled to 2 µK to measure the magnetic field with and without compensation. We set the quantization axis to be the x-axis, with the quantization field $B_x = 200$ kHz$/\gamma = 286$ mG, where $\gamma = 700$ kHz/G is the gyromagnetic ratio of ^{87}Rb in the F = 1 manifold. The atoms were prepared through the following sequence [5]. First, an incoherent optical pumping brought the atoms to the $|F = 1, m_F = 1\rangle$ dark state, which in the basis of the $|F = 1\rangle$ sublevel states $(\psi_{+1}, \psi_0, \psi_{-1})^T$, quantized along the x-axis, is written as $(1, 0, 0)_x^T$, with the subindex x indicating the basis. Then a $\pi/2$-RF pulse of 200 kHz along the z-axis was applied to rotate the spin state to the state

$$e^{-i\frac{\pi}{2}\hat{F}_z}\cdot\begin{pmatrix}1\\0\\0\end{pmatrix}_x=\exp\left(-i\frac{\pi}{2}\frac{1}{\sqrt{2}}\begin{pmatrix}0&-i&0\\i&0&-i\\0&i&0\end{pmatrix}_x\right)\cdot\begin{pmatrix}1\\0\\0\end{pmatrix}_x=\begin{pmatrix}1/2\\1/\sqrt{2}\\1/2\end{pmatrix}_x.$$

Due to the external field the state evolves as $|\psi\rangle = e^{-i\hat{H}t/\hbar}\cdot(1/2, 1/\sqrt{2}, 1/2)^T_x = (1/2\cdot e^{-i\omega t}, 1/\sqrt{2}, 1/2\cdot e^{i\omega t})^T_x$, perpendicular to the x-axis and precessing at Larmor frequency ω due to B_x field that generates a Hamiltonian $\hat{H} = \mu_B g_F \hat{\vec{B}}\cdot\hat{\vec{F}} = \mu_B g_F \hat{B}_x\cdot\hat{F}_x = \hbar\omega\cdot\mathrm{diag}(1,0,-1)_x$, where μ_B is the Bohr magneton, g_F is the hyperfine Landé g-factor [6], and we define $\omega = \mu_B g_F B_x/\hbar$.

Next, we measured the polarization rotation angle ϕ on the Poincaré sphere using Faraday probe. According to [20], for a single atom this is

$$\begin{aligned}\langle\phi\rangle &= G_1\cdot\langle\hat{F}_z\rangle = G_1\cdot\langle\psi|\hat{F}_z|\psi\rangle\\ &= G_1\cdot\left(\tfrac{1}{2}e^{i\omega t}\quad\tfrac{1}{\sqrt{2}}\quad\tfrac{1}{2}e^{-i\omega t}\right)_x\cdot\frac{1}{\sqrt{2}}\begin{pmatrix}0&-i&0\\i&0&-i\\0&i&0\end{pmatrix}_x\cdot\begin{pmatrix}\frac{1}{2}e^{-i\omega t}\\\frac{1}{\sqrt{2}}\\\frac{1}{2}e^{i\omega t}\end{pmatrix}_x = G_1\sin\omega t,\end{aligned}$$

where G_1 is the vectorial atom light coupling factor. Hence, for an ensemble of N_{atoms} atoms we have $\langle\phi\rangle = G_1\sin\omega t\cdot N_{atoms}$.

For each Faraday rotation measurement we held and retriggered the measurement start point to synchronize with the 50 Hz signal. Then we performed state rotation with $\pi/2$-RF pulse and let the system evolve for a hold time τ. We measured the Faraday rotation frequency ω, which is directly related with the instantaneous magnetic field through the gyromagnetic ratio γ. In this way we could reconstruct the field's shape from its values measured using different hold times. On the other hand, the instantaneous phase $\theta = \omega t$ is proportional to the time integral of the magnetic field within the time window from 0 to τ, hence its standard deviation gives us an insight of how repeatable the magnetic field is from experiment to experiment.

5. Results

We generated artificial background magnetic field noise (with frequency multiples of 50 Hz), using the passive control coils, to test the noise reduction capability of our compensator. Fig. 5 plots the reduction as the ratio in dB of the standard deviations of the noise with and without compensation, measured by the fluxgate sensor (in-loop measurement), versus noise frequency. The noise was suppressed by 24 dB (factor 15) at 50 Hz, 18 dB (factor 8) at 100 Hz, and 15 dB (factor 6) at 150.

Afterwards, with the artificial noise turned off, we performed Faraday rotation measurements for hold times ranging from 20 µs to 100 ms, under the same lab conditions

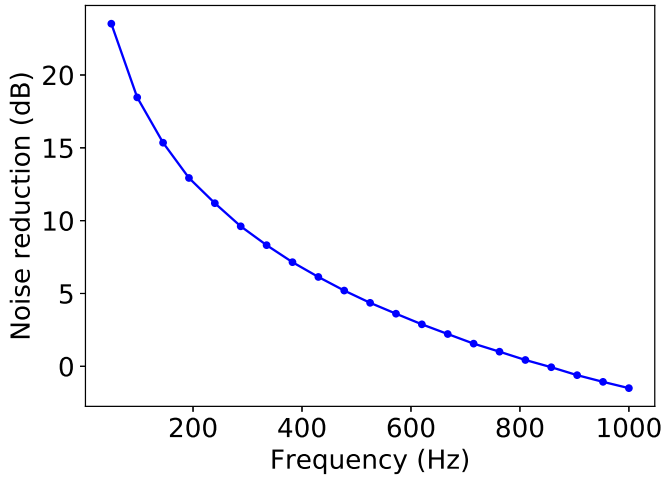

Figure 5: Noise reduction with compensation turned on.

between them. In this way we could evaluate the performance of our compensator against the magnetic field noise in the lab. The standard deviation of θ versus hold time is shown in Fig. 6.

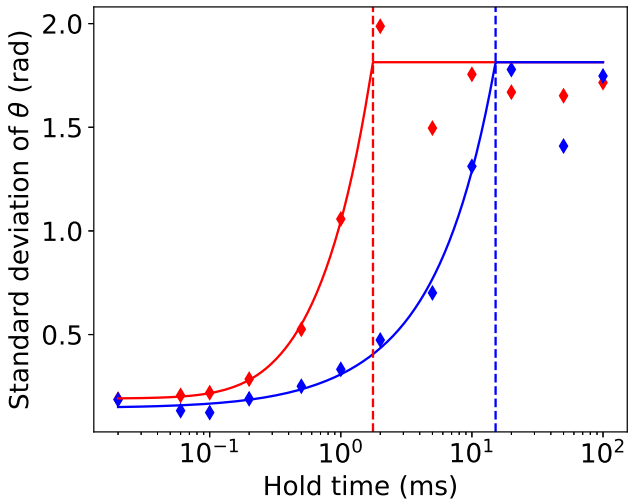

Figure 6: Standard deviation of the instantaneous phase with (blue) and without (red) compensation. The model for data fitting is $\sigma(\theta) = \sqrt{\sigma_0^2 + A^2 \cdot \tau + B^2 \cdot \tau^2}$ with the condition $\sigma(\theta) \leq \pi/\sqrt{3}$, which is the maximum standard deviation we can have for a random variable uniformly distributed from 0 to 2π. The B^2t^2 term accounts for changes in the magnetic DC field between different experimental runs. The term $A^2 \cdot \tau$ assumes that there is an extra random-walk type of noise which adds to the measurement. This gives a variances proportional to the number of measurement N, which is proportional to τ. The constant bias variance σ_0^2 is due to the inherent uncertainty in the state preparation and atomic readout.

The trend is that the instantaneous phase has low standard deviation with short hold times, and increases as the integral of the magnetic field becomes larger with longer hold times, ultimately reaching the maximum value of $\pi/\sqrt{3}$. At this point different phase measurements under the same conditions would yield an outcome which could be any value between 0 to 2π, so the measurement is no longer repeatable. Therefore we can say that the field measurement is repeatable up to 15.2 ms ($\delta B_x = 94\,\mu\text{G}$), while it is up to 1.8 ms ($\delta B_x = 812\,\mu\text{G}$) without compensation. As to the field stability, we measured the Larmor frequency of the atoms for a hold time up to 20 ms (Fig. 7), that is, a whole sycle of the 50 Hz signal. As expected, the frequency remains around 200 kHz, but makes fluctuations of 1.2 kHz peak-to-peak (1.7 mG) without compensation and 270 Hz peak-to-peak (0.38 mG) with compensation, fulfilling the requirement for our atomic physics experiments.

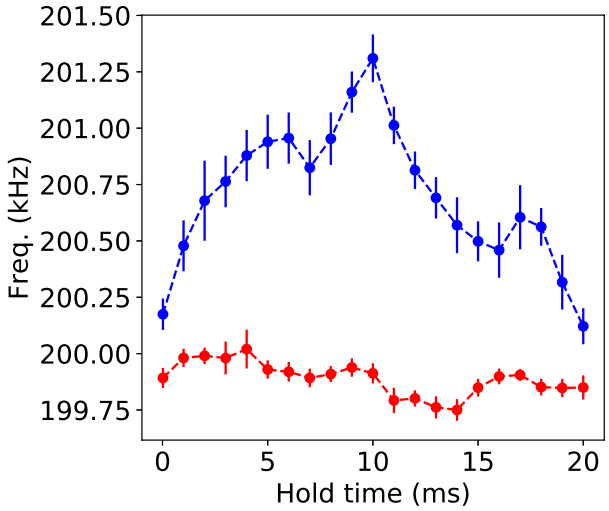

Figure 7: Frequency stability mean with (blue) and without (red) compensation, corresponding to a whole cycle of the 50 Hz field.

6. Conclusions and outlook

We built and tested a magnetic field compensator with closed-loop control. Its overall performance fulfills the noise level requirement ($\leq$ 1 mG) for our atomic physics experiments, achieving a stability of $\leq$ 0.4 mG. The system also yields satisfactory repeatability, being better than 100 µG. Compensation for the other two axes will also be implemented in the future using the same scheme developed in this project.

Acknowledgements

The author wants to acknowledge the following people for the help and advices received during the project's development: Morgan Mitchell, Silvana Palacios, Simon Coop, Robert Sewell, and mostly, Pau Gómez. The author is also grateful to the work done by Tobias Klafka [12] which served as a source of inspiration. And as always, thanks to be expressed to his parents and girlfriend for their constant support.

References

[1] M-S Chang et al. Observation of spinor dynamics in optically trapped rb 87 bose-einstein condensates. *Physical review letters*, 92(14):140403, 2004.

[2] D. Sheng et al. Subfemtotesla scalar atomic magnetometry using multipass cells. *Physical review letters*, 110(16):160802, 2013.

[3] V. G. Lucivero et al. Shot-noise-limited magnetometer with sub-picotesla sensitivity at room temperature. *Review of Scientific Instruments*, 85(11):113108, 2014.

[4] B. Pasquiou. *Effets de linteraction dipôle-dipôle sur les propriétés magnétiques dun condensat de chrome*. PhD thesis, Université Paris-Nord, November 2011.

[5] S. Palacios et al. Multi-second magnetic coherence in a single domain spinor bose-einstein condensate. *arXiv preprint arXiv:1707.09607*, 2017.

[6] D. A. Steck. Rubidium 87 d line data, 2001.

[7] H. Youk. Numerical study of quadrupole magnetic traps for neutral atoms: anti-helmholtz coils and a u-chip. *Canadian Undergraduate Physics Journal*, 3(2):13–18, 2005.

[8] C. J. Dedman et al. Active cancellation of stray magnetic fields in a bose-einstein condensation experiment. *Review of scientific instruments*, 78(2):024703, 2007.

[9] Bartington Instruments. *Operation Manual for Mag-03 Three-Axis Magnetic Field Sensors*. OM1004/28.

[10] A. Matsuoka et al. Development of fluxgate magnetometers and applications to the space science missions. *An Introduction to Space Instrumentation*, pages 217–225, 2013.

[11] F. Primdahl. The fluxgate magnetometer. *Journal of Physics E: Scientific Instruments*, 12(4):241, 1979.

[12] T. Klafka. Towards active magnetic field compensation for ultracold atom experiments. Master's thesis, Universität Hamburg, November 2016.

[13] A. Sheikholeslami. Source degeneration [circuit intuitions]. *IEEE Solid-State Circuits Magazine*, 6(3):5–6, 2014.

[14] Vishay Siliconix. *Datasheet of E Series Power MOSFET*, October 2012.

[15] O. Baltag et al. Dynamic shielding of the magnetic fields. *Advances in Electrical and Computer Engineering*, 10(4):135–142, 2010.

[16] M. E. Rudd et al. Optimum spacing of square and circular coil pairs. *Review of Scientific Instruments*, 39(9):1372–1374, 1968.

[17] L. A. Marzetta. Use of an operational amplifier with helmholtz coils for reducing ac induced magnetic fields. *Review of Scientific Instruments*, 32(11):1192–1195, 1961.

[18] Digilent. *chipKIT uC32 Board Reference Manual*, December 2014.

[19] Digilent. *Analog Shield Reference Manual*, June 2014.

[20] M. Koschorreck et al. Sub-projection-noise sensitivity in broadband atomic magnetometry. *Physical review letters*, 104(9):093602, 2010.